Vibrational Properties of Calcium Phosphate Compounds. 2. Comparison between Hydroxyapatite and β-Tricalcium Phosphate

P. N. de Aza, F. Guitián, and C. Santos

Instituto de Cerámica, Universidad de Santiago de Compostela, 15706 Santiago de Compostela, Spain

S. de Aza

Instituto de Cerámica y Vidrio, Consejo Superior de Investigaciones Científcas (CSIC), Arganda del Rey, Madrid, Spain

R. Cuscó* and L. Artús

Institut Jaume Almera, Consell Superior d'Investigacions Científques (CSIC), Lluís Solé i Sabarís s.n., 08028 Barcelona, Spain

Received August 9, 1996. Revised Manuscript Received January 30, 1997[⊗]

A comparison between Raman spectra of polycrystalline $Ca_{10}(PO_4)_6(OH)_2$ and β-$Ca_3(PO_4)_2$ is reported. Both compounds exhibit similar Raman spectra, which are dominated by the internal modes of the PO_4^{3-} tetrahedra. However, several characteristic features of the Raman spectra allow us to establish a distinction between these two calcium phosphates. Besides the presence of peaks associated with vibrations of the OH^- group in the Raman spectrum of hydroxyapatite, which are highly sensitive to sample crystallinity, other characteristic features such as the width of the PO_4^{3-} internal bands can be used to distinguish between hydroxyapatite and β-$Ca_3(PO_4)_2$.

I. Introduction

Hydroxyapatite (HA, $Ca_{10}(PO_4)_6(OH)_2$), one of the primary constituents of bone and teeth, and β-tricalcium phosphate (TCP, $Ca_3(PO_4)_2$) were the first ceramic biomaterials used in prosthetic implants. During the synthesis of HA, depending on pH conditions, Ca/P ratio, aging time, and temperature of the thermal treatment, variable quantities of TCP can be produced.[1] HA is bioactive and joins directly to the bone tissue while TCP is resorbable.[2−4] Raman spectroscopy can be used as a nondestructive technique to properly differentiate both calcium phosphates, even when the degree of crystallinity of the samples is not very high.

On the other hand, leaving aside the calcium phosphate ceramics, the formation of a HA layer on the surface of other bioactive materials when they are soaked in an acellular simulate body fluid (SBF) has a significant influence on their subsequent bonding with bone tissue (bioactivity) when they are implanted in a living body.[5,6] Micro-Raman spectroscopy can also be used as a nondestructive probe to analyze the structural changes with spatial resolution down to ≈1 μm. Quite recently, micro-Raman measurements were performed in order to gain information about the structure of the bone-implant interface with spatial resolution of ≈5 μm.[7]

A good knowledge of the vibrational properties of HA and β-TCP may help to establish a clear identification of these two calcium phosphates. Although the Raman activity of the OH^- group of HA would apparently suffice to establish the difference between HA and TCP, in practice the detection of the most characteristic OH^- mode due to the O−H bond stretching vibration at ≈3576 cm^{-1} (ref 8) is difficult in samples where the degree of crystallinity is not very high. Therefore, the knowledge of other differential features in the Raman spectra of HA and TCP is desirable in order to identify these two forms of calcium phosphate.

The crystal structure of HA was determined by neutron[9] and X-ray diffraction,[10] and a study of its phonon spectrum by means of polarized Raman scattering has also been reported.[11] The phonon spectrum of fluorapatite (FA), another member of the apatite group closely related to HA, which is obtained by the replacement of the OH^- ions of the HA structure by F^- ions in a very close but higher symmetry position, has been extensively studied, both theoretically through a polarizable ion model,[12] and experimentally by means

[⊗] Abstract published in *Advance ACS Abstracts,* March 1, 1997.

(1) Santos, C. Ph.D. Thesis, University of Santiago de Compostela, Spain, 1994.
(2) Hench, L. L.; Clark, A. E. In *Biocompatibility of Orthopaedic Implants*; Williams, D. F., Ed.; CRC Press: Boca Raton, FL, 1982.
(3) Hench, L. L. In *Bioceramics*; Ducheyne, P., Lemons, J., Eds.; Annals N.Y. Acad. Sci. 1988; Vol. 523, p 54.
(4) De Groot, K. In *Bioceramics of calcium phosphate*; De Groot, K., Ed.; CRC Press: Boca Raton, FL, 1983.
(5) Hench, L. L. *J. Am. Ceram. Soc.* **1991**, *74*, 1487.
(6) Ohtsuki, C.; Kokubo, T.; Yamamuro, T. *J. Non-Cryst. Solids* **1992**, *143*, 84.
(7) Leung, Y. C.; Walters, M. A.; Blumenthal, N. C.; Ricci, J. L.; Spivak, J. M. *J. Biomed. Mater. Res.* **1995**, *29*, 591.
(8) Fowler, B. O. *Inorg. Chem.* **1974**, *13*, 194.
(9) Kay, M. I.; Young, R. A.; Posner, A. S. *Nature* **1964**, *204*, 1050.
(10) Elliot, J. C.; Mackie, P. E.; Young, R. A. *Science* **1973**, *180*, 1055.
(11) Iqbal, Z.; Tomaselli, V. P.; Fahrenfeld, O.; Möller, K. D.; Ruszala, F. A.; Kostiner, E. *J. Phys. Chem. Solids* **1977**, *38*, 923.
(12) Devarajan, V.; Klee, W. E. *Phys. Chem. Miner.* **1981**, *7*, 35.

S0897-4756(96)00426-7 CCC: $14.00

of Raman scattering measurements.[13−15] The crystal structure of β-TCP was determined by X-ray diffraction measurements.[16] In the preceding work,[17] hereafter referred to as paper 1, we reported a study of the Raman spectrum of polycrystalline β-TCP over the whole optical frequency range.

In this paper we present high-resolution room-temperature Raman scattering measurements on polycrystalline HA and compare the Raman spectra of HA and β-TCP. Characteristic differences in the Raman spectra of HA and β-TCP are related to their respective crystallographic structures. In particular, we discuss the differences between the Raman spectra of HA and β-TCP with the aid of a dynamical model of the PO_4^{3-} ion which we have developed to explain the basic trends observed in the regions of the Raman spectra corresponding to the internal PO_4^{3-} modes of both compounds as well as the role of tetrahedra distortion in the frequency shifts relative to the free ion.

II. Experimental Section

Pure polycristalline HA was obtained at room temperature by stoichiometric reaction of 0.431 M $Ca(NO_3)_2$ and 0.258 M H_3PO_4 solutions at pH = 11 in a closed reactor with continuous stirring, leaving the precipitate to age for 1 day also with continuous stirring. After drying at 110 °C for 24 h, the precipitate was isostatically pressed into pellets which were subsequently heated in air atmosphere in an electric furnace at a rate of 5 °C/min to 800 °C. The samples were maintained at this temperature for 1 h, with a water vapor pressure of 10 mmHg, before being furnace cooled. The Ca/P molar ratio of these samples was determined by ICP-AES and found to be 1.67 ± 0.01. X-ray diffraction analysis revealed the presence of only the HA phase. To check the effects of sample crystallinity on the Raman spectra, and the stability of the OH^- group in the HA structure, some pellets of HA precipitate were heated at 600, 1000, and 1300 °C for 1 h. After thermal treatments, X-ray diffraction analysis were carried out to check that no other phosphate phases were present in the HA samples.

The Raman scattering measurements were performed using a Raman microprobe instrument consisting of a Jobin-Yvon T64000 spectrometer equipped with a microscope which allows a spatial resolution on the sample close to 1 μm. The Raman signal was detected by a multichannel CCD detector cooled with liquid nitrogen. The Raman spectra were recorded using the triple additive configuration of the spectrometer, with a spectral resolution better than 1 cm^{-1}. The light was collected in backscattering geometry through an objective of numerical aperture 0.95. The 488-nm line of an Ar^+ laser was used as excitation, focused in a spot of ≈1 μm in diameter, with an incident power on the sample of ≈2 mW. Due to the polycrystalline nature of the samples studied the Raman spectra were recorded without polarization analysis.

III. Results and Discussion

A. Raman Spectrum of HA. To establish a closer comparison with the Raman spectrum of polycrystalline β-TCP discussed in paper 1, we performed high-resolution Raman scattering measurements on polycrystalline HA. The room-temperature Raman spectrum of polycrystalline HA over the whole optical frequency range, obtained from the sample treated at 800 °C, is shown in Figures 1a and 2a. As in the case of FA,[12−15] the Raman spectrum of HA is dominated by the internal PO_4^{3-} modes. The vibrational frequencies of the free PO_4^{3-} were found to be ν_1 = 938 cm^{-1}, ν_2 = 420 cm^{-1}, ν_3 = 1017 cm^{-1}, and ν_4 = 567 cm^{-1} by means of Raman scattering measurements on phosphates in aqueous solutions.[18] These frequencies correspond, respectively, to the symmetric P−O stretching mode, the doubly degenerate O−P−O bending modes, the triply degenerate asymmetric P−O stretching modes, and the triply degenerate modes of mainly O−P−O bending character. As discussed in paper 1, site symmetry and correlation effects induce energy shifts and splittings of the PO_4^{3-} modes relative to the free ion. In the Raman spectrum of HA shown in Figure 1a, well-defined bands centered around frequencies 21−25 cm^{-1} higher than those of the

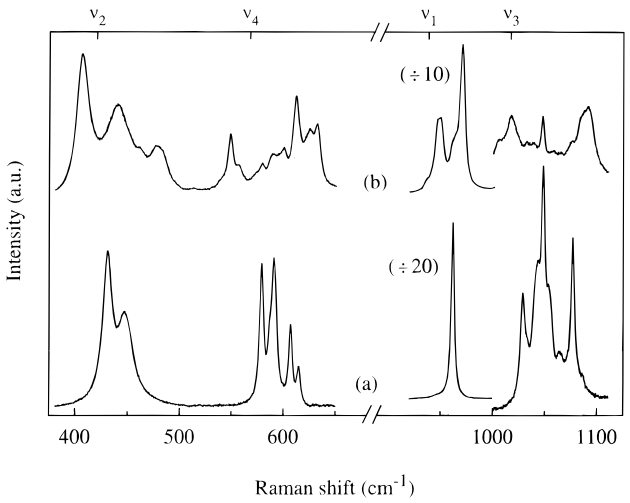

Figure 1. Comparison between the Raman spectra of (a) HA and (b) β-TCP in the frequency regions corresponding to the internal PO_4^{3-} modes. The intensity scale is the same for both spectra.

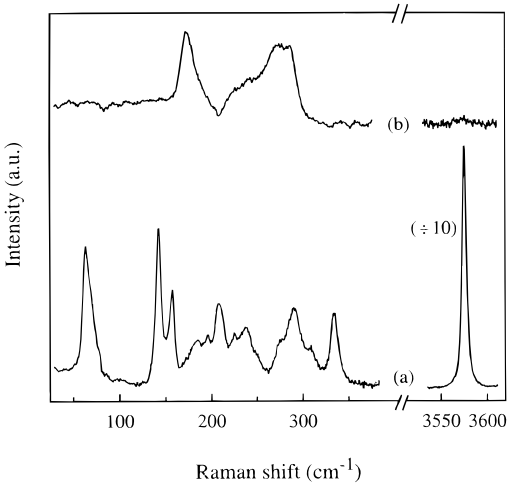

Figure 2. Comparison between the Raman spectra of (a) HA and (b) β-TCP in the frequency regions corresponding to external lattice modes and O−H stretching vibration. The intensity scale is the same for both spectra. The intensity ratio between the O−H stretching peak at 3576 cm^{-1} and the ν_1 peak of HA at 962 cm^{-1} shown in Figure 1 is 0.22.

(13) Kravitz, L. C.; Kingsley, J. D.; Elkin, E. L. *J. Chem. Phys.* **1968**, *49*, 4600.
(14) Boyer, L. L.; Fleury, P. A. *Phys. Rev. B* **1974**, *9*, 2693.
(15) Adams, D. M.; Gardner, I. R. *J. Chem. Soc., Dalton* **1974**, 1505.
(16) Dickens, B.; Schroeder, L. W.; Brown, W. E. *J. Solid State Chem.* **1974**, *10*, 232.
(17) de Aza, P. N.; Santos, C.; Pazo, A.; de Aza, S.; Cuscó, R.; Artús, L. *Chem. Mater.* preceding paper in this issue.
(18) Nakamoto, K. *Infrared and Raman Spectra of Inorganic Coordination Compounds*; John Wiley & Sons: New York, 1986; p 138.

Table 1. Factor Group Analysis (C_6) of the Internal Modes of the PO_4^{3-} Tetrahedra in HA[a]

free PO_4^{3-} tetrahedron		PO_4^{3-} tetrahedra in HA crystal		
internal modes	T_d symmetry	no. of modes	C_1 site symmetry	C_6 factor group symmetry
ν_1	$A_1^{(R)}$	6	$6(A^{(RI)})$	$A^{(RI)} + B^{(0)} + E_1^{(RI)} + E_2^{(R)}$
ν_2	$E^{(R)}$	12	$6(2A^{(RI)})$	$2A^{(RI)} + 2B^{(0)} + 2E_1^{(RI)} + 2E_2^{(R)}$
ν_3	$T_2^{(RI)}$	18	$6(3A^{(RI)})$	$3A^{(RI)} + 3B^{(0)} + 3E_1^{(RI)} + 3E_2^{(R)}$
ν_4	$T_2^{(RI)}$	18	$6(3A^{(RI)})$	$3A^{(RI)} + 3B^{(0)} + 3E_1^{(RI)} + 3E_2^{(R)}$

[a] (RI) = Raman and infrared active, (R) = Raman active, (0) = inactive.

corresponding free PO_4^{3-} modes can be observed. On the basis of the correspondence between the observed bands and the free PO_4^{3-} ion frequencies, the strong peak observed in Figure 1a at 962 cm^{-1} is assigned to symmetric stretching modes, and the bands observed in the frequency regions 400−490, 570−625, and 1020−1095 cm^{-1} are assigned, respectively, to ν_2-, ν_4-, and ν_3-type internal PO_4^{3-} modes, in agreement with ref 11. Furthermore, polarizable ion model calculations for FA,[12] whose internal PO_4^{3-} frequencies are not expected to be far from those of HA, yield internal mode frequencies in excellent agreement with the Raman scattering bands which we have observed in HA.

The HA crystallizes in the $P6_3/m$ space group, and its unit cell contains six PO_4^{3-} tetrahedra. According to neutron diffraction data,[9] the P−O bond lengths of the PO_4^{3-} tetrahedra in the HA structure range from 1.529 to 1.547 Å, and the O−P−O angles from 107.5° to 111.5°. Although a slight distortion of the tetrahedra is probable, given the standard deviation of the neutron results the differences in P−O bond length obtained from neutron diffraction data are not considered significant.[9]

Taking into account that each tetrahedron contributes 9 internal vibrational modes,[19] 54 internal PO_4^{3-} modes are expected in HA, which are split by the HA crystal field as shown in Table 1. C_1 site symmetry lifts the degeneracy of the doubly degenerate ν_2 and the triply degenerate ν_3 and ν_4 modes of the tetrahedron and leads to six identical sets of nine different frequencies. C_6 factor group symmetry further splits each of these frequencies as shown on the fifth column of Table 1. The predicted multiplicity of Raman lines for each band was observed in the polarized measurements of Iqbal et al.,[11] although some of the peaks were very weak and degenerate within experimental resolution, and the possibility of incomplete extinction of some of the modes forbidden by selection rules makes difficult in some cases their unambiguous identification. Modes arising from the degenerate normal modes of the tetrahedron but belonging to different representations of the factor group of the crystal are degenerate or lie very close in energy. For instance, the HA internal modes arising from the doubly degenerate ν_2 normal modes of the tetrahedron are split by ≈17 cm^{-1} in the A and E_2 representations and by ≈10 cm^{-1} in the E_1 representation, but the lowest energy mode for each representation is found at ≈433 cm^{-1}. This precludes the resolution in polycrystalline samples of all the modes predicted by group theory. However, as can be seen in Table 2, where we list the frequency positions of the peaks and shoulders observed in our unpolarized spectra, a good correlation is found with the values reported in ref 11.

Table 2. Frequencies (cm^{-1}) of the Observed Raman Peaks of Polycrystalline β-TCP and HA Associated with PO_4^{3-} Internal Modes

ν_1			ν_2			ν_3			ν_4		
TCP	HA	HA[a]	TCP	HA	HA[a]	TCP	HA	HA[a]	TCP	HA	HA[a]
946			405			1005			547		
949				430		1016			555		
961					432			1028	578		
	962	962			433		1029	1029		579	
		963	439			1031					580
970					443		1033	1033			581
				447		1038			588	588	588
					449		1043	1043		591	
					450	1046		1046			592
			460	452			1048			594	594
			475				1054	1054	599		
			483			1059					606
						1074		1074		607	608
							1077	1076	611		
						1084				615	
						1091					617
									624		
									631		

[a] Reference 11.

The OH^- group has C_3 site symmetry in the HA lattice. Its stretching mode, belonging to the A_1 representation of C_3, is split by the crystal field into the A and B representations of C_6, of which only A is Raman active. As can be seen in Figure 2a, a strong Raman peak is observed at 3576 cm^{-1} corresponding to the OH^- stretching mode. The same mode was detected in IR measurements and unambiguously assigned to OH^- on the basis of deuteration shifts.[8] We note that the intensity of this peak is strongly dependent on the crystallinity of the samples. For instance, whereas the intensity and the width of the ν_1 peak were the same for HA samples thermally treated at 600 and 800 °C, the intensity of the O−H stretching mode was about 3 times higher for the samples treated at 800 °C. In samples treated at higher temperatures a progressive crystallinity degradation is observed, as reflected by the increasing width of the Raman peaks and a substantial intensity reduction of the O−H stretching peak. So, the highest degree of crystallinity of the HA samples appears to be achieved after calcination at around 800 °C. A peak at 343 cm^{-1} and a shoulder at about 355 cm^{-1} were found by infrared measurements[8] and assigned to Ca−(OH) sublattice motion on the basis of isotopic substitution shifts. In Figure 2a, we observe a Raman peak at 335 cm^{-1} which we attribute to the OH^- translational modes. In fact, in the samples treated at 800 °C the intensity of this peak is about 4 times higher than in the samples treated at 600 °C, showing a correlation with the intensity of the O−H stretching mode at 3576 cm^{-1} which supports this assignment, in agreement with refs 8 and 11. The OH^- librational mode was located at 630 cm^{-1} by infrared measurements.[8] We could not detect any Raman peak around this frequency, confirming the previous Raman measurements of Iqbal et al.[11] However, we have observed that the peak at 615 cm^{-1}, which in ref 11 was assigned to an internal mode although the OH^- librational modes were also allowed in the same polarization configuration, tends to disappear in the samples calcined at 1300

(19) Herzberg, G. *Molecular Spectra and Molecular Structure II. Infra-Red and Raman Spectra of Polyatomic Molecules*; D. Van Nostrand: Princeton, 1945.

°C. Thus, the possibility of this peak corresponding to an OH^- librational mode should not be ruled out.

Following the results of the extensive infrared study of isotopic substitution in hydroxyapatites by Fowler,[8] and also taking into account the results of the model calculations for FA,[12] we associate the Raman lines below 320 cm^{-1} with vibrational modes involving translational motion of the Ca^{2+} and PO_4^{3-} sublattices, and with librational modes of the PO_4^{3-} ion. In Figure 2a, a distinct peak can be seen at 65 cm^{-1}. Iqbal et al.[11] also observed a peak at this frequency in HA and a corresponding peak at 45 cm^{-1} in FA. They related the large frequency shift of this mode in these two compounds to the different crystal potential, but the assignment of these peaks was not made. According to the calculations of Devarajan and Klee[12] the peak observed by Adams and Gardner[15] in FA at about 44 cm^{-1} could be associated with translational vibrations of the Ca^{2+} sublattice. Further experimental and theoretical work will be necessary to determine unambiguously the nature of this low-frequency mode in HA crystals.

B. Comparison between the Raman Spectra of *β*-TCP and HA. *1. PO_4^{3-} Internal Modes.* The *β*-TCP and HA crystals exhibit a strong molecular character as regards to their vibrational properties, and their Raman spectra are dominated by the internal PO_4^{3-} bands. In Figure 1 we compare the high-resolution spectra of *β*-TCP and HA in the frequency regions of the phosphate internal modes. As can be seen from Figure 1, for both *β*-TCP and HA the internal PO_4^{3-} bands are centered around the same frequency values, about 20 cm^{-1} above the corresponding free PO_4^{3-} frequencies, suggesting the existence of strong site fields in both crystals which reduce the interatomic distances and therefore stiffen the intratetrahedral bonds in relation to the free ion. It is also apparent from Figure 1 that *β*-TCP internal bands span a wider frequency range than the corresponding HA internal bands. In particular, it should be noted that while in HA the Raman-active ν_1 modes ($A + E_1 + E_2$) are degenerate within the experimental resolution, and a single peak at 961 cm^{-1} is detected, in *β*-TCP, besides the main peak observed at 971 cm^{-1}, other frequencies are detected forming a broad peak at 946−949 cm^{-1} and a shoulder at 961 cm^{-1}. As the internal bands are centered at about the same frequency values for both *β*-TCP and HA, the wider frequency range of the *β*-TCP ν_2- and ν_4-type modes makes these two bands to appear very close together in the *β*-TCP spectrum, whereas they are well separated in HA. This is a characteristic feature of the Raman spectra which allows to distinguish between *β*-TCP and HA even in samples of lesser quality where it is difficult to resolve individual peaks in the bands.

As discussed in paper 1, the shifts and splittings of the internal PO_4^{3-} frequencies are due to site and correlation effects. Site effects, which include deformations of the PO_4^{3-} tetrahedra due to the site field induced by the surrounding ions, are expected to produce larger shifts and splittings of the internal modes in *β*-TCP because, as revealed by neutron and X-ray diffraction measurements,[9,16] the distortion of the PO_4^{3-} tetrahedra is higher in *β*-TCP than in HA. In fact, whereas in *β*-TCP intratetrahedral O−P bond lengths range from 1.498 to 1.548 Å, and O−P−O angles from 104.9° to 115.9°, in HA intratetrahedral O−P bond lengths range from 1.529 to 1.547 Å, and O−P−O angles from 107.5° to 111.5°. Furthermore, whereas the six PO_4^{3-} tetrahedra of the HA unit cell are crystallographically equivalent, three different types of crystallographically nonequivalent PO_4^{3-} tetrahedra can be distinguished in the far more complex *β*-TCP structure.

It is seen in Figures 1 and 2 that individual peaks are significantly broader in *β*-TCP than in HA. Two reasons may contribute to the increased width of the *β*-TCP peaks. On the one hand, as we have already discussed, taking into account the large number of modes supported by the *β*-TCP unit cell the participation in a given Raman peak of modes very close in energy is very likely. On the other hand, the *β*-TCP crystal contains cation sites with half occupancy[16] which contribute to disorder in the structure.

2. Modeling the Effect of PO_4^{3-} Tetrahedra Distortion. The effect of tetrahedra distortion on the internal mode frequencies of *β*-TCP and HA can be estimated from the change in force constants associated with variations of the different intratetrahedral bond lengths. The normal modes of a general molecular unit can be obtained using standard methods of the classical theory of small oscillations once the potential energy of the molecule has been set up. Dennison[20] proposed a model to calculate the normal modes of the tetrahedral methane molecule based on a field of central forces around each nucleus, which has subsequently been considered for modeling vibrational modes in other tetrahedral molecules.[19,21] This model rests upon the assumption that, for small displacements of the nuclei, the symmetrical distribution of the electronic charge around each ion is not significantly distorted so that the electrostatic forces between each pair of ions remain central. The central force assumption works quite well for halides of C and Si but is rather poor for other molecular units, including the PO_4^{3-} ion.[19] The neglect of three-body potentials depending on bond-angle variations constitutes a serious limitation to the model. On the other hand, the Keating model[22,23] has been successful in explaining the lattice dynamics of standard semiconductor crystals, in which the bond is mainly covalent, using a small number of adjustable parameters which have a direct physical interpretation as bond stretching and bond bending force constants. However, the Keating model cannot be directly applied to the PO_4^{3-} molecular ion because the ionic character of its constituents leads to nonvanishing electrostatic forces between pairs of atoms in the equilibrium position, contrary to the Keating model forces which depend only on displacements of the atoms relative to the equilibrium position. To overcome the limitations of these two different approaches for the present case, we have set up a model in which the potential energy is written as a sum of central field interactions between pairs of atoms and Keating-type bond-bending interactions depending on the O−P−O angles. In the central field interactions we include the electrostatic forces between the ions in the tetrahedron, which do not vanish at equilibrium, and the short-range intratetrahedral forces corresponding to the bond stretch-

(20) Dennison, D. M. *Astrophys. J.* **1925**, *62*, 84.
(21) Scott, J. F. *J. Raman Spectrosc.* **1989**, *20*, 123.
(22) Keating, P. N. *Phys. Rev.* **1966**, *145*, 637.
(23) Kane, E. O. *Phys. Rev. B* **1985**, *31*, 7865.

ing potentials of the Keating model. The departure from the central field assumptions is accounted for by the Keating bond bending interaction. Therefore, in our model, the total potential energy of the PO_4^{3-} group can be expanded up to quadratic terms as

$$\phi(\mathbf{r}_i - \mathbf{r}_j) = \phi_0 + \sum_{n=1}^{4}\frac{\partial\phi}{\partial\rho_n}\rho_n + \frac{1}{2}\sum_{n=1}^{4}\frac{\partial^2\phi}{\partial{\rho_n}^2}{\rho_n}^2 + \sum_{n=1}^{6}\frac{\partial\phi}{\partial q_n}q_n + \frac{1}{2}\sum_{n=1}^{6}\frac{\partial^2\phi}{\partial{q_n}^2}{q_n}^2 + \frac{3}{4}\sum_{\substack{n,m\\ n>m=1}}^{4}\beta_{nm}[(\mathbf{r}_n - \mathbf{r}_0)\cdot\hat{\mathbf{R}}_m + (\mathbf{r}_m - \mathbf{r}_0)\cdot\hat{\mathbf{R}}_n]^2 \quad (1)$$

where ρ_i are the radial displacements of the oxygen relative to the phosphorus, q_i are the mutual displacements of the oxygen atoms relative to each other, $\mathbf{r}_n$ are the Cartesian vectors giving the displacements of the nuclei from their equilibrium positions, $\hat{\mathbf{R}}_n$ are the unit vectors pointing to the equilibrium positions, and β_{nm} are the Keating bond-bending force constants associated with the O(n)−P−O(m) angles. The normal modes of vibration are obtained by diagonalization of the dynamical matrix

$$D_{m,n;i,j} = \frac{1}{\sqrt{M_m M_n}}\frac{\partial^2\phi}{\partial(\mathbf{r}_m)_i\,\partial(\mathbf{r}_n)_j} \quad (2)$$

In the regular tetrahedron, symmetry considerations allow us to set $(1/d_{PO})\partial\phi/\partial\rho_i = k'_{PO}$, $(1/d_{OO})\partial\phi/\partial q_i = k'_{OO}$, $\partial^2\phi/\partial\rho_i^2 = k_{PO}$, and $\partial^2\phi/\partial q_i^2 = k_{OO}$ (for all i), and $\beta_{mn} = \beta$ (for all m, n). d_{PO} and d_{OO} denote, respectively, the equilibrium P−O and O−O distances, which are incorporated in the definitions of k'_{PO} and k'_{OO} so that these quantities have the dimensions of a force constant. Further, the static equilibrium conditions impose the relation $k'_{PO} = -\sqrt{6}k'_{OO}$, and therefore the potential energy (eq 1) contains only four independent adjustable parameters: k'_{PO}, k_{PO}, k_{OO}, and β. A least-squares fit to the experimental frequencies $\nu_1 = 938$ cm^{-1}, $\nu_2 = 420$ cm^{-1}, $\nu_3 = 1017$ cm^{-1}, and $\nu_4 = 567$ cm^{-1} of the PO_4^{3-} ion in aqueous solution yields $k'_{PO} = 2.22 \times 10^4$ dyn/cm, $k_{PO} = 5.23 \times 10^5$ dyn/cm, $k_{OO} = 7.37 \times 10^4$ dyn/cm, and $\beta = 2.22 \times 10^4$ dyn/cm. In a distorted tetrahedron, the partial derivatives appearing in eq 1 as well as the β_{mn} coefficients will be different, giving rise to different force constants specific to each pair of atoms and each O−P−O angle. For covalent tetrahedral bonds, Harrison[24] showed that the dependence on the bond length for the bond-stretching force constants scaled as d^{-4}. Experimental studies of the optical phonon energy dependence in tetrahedrally coordinated group IV semiconductor[25] and other cubic compounds,[26] as well as in II−IV−V_2 chalcopyrite compounds,[27] have shown a fairly good agreement with Harrison's prediction. This model has also been successfully applied to predict

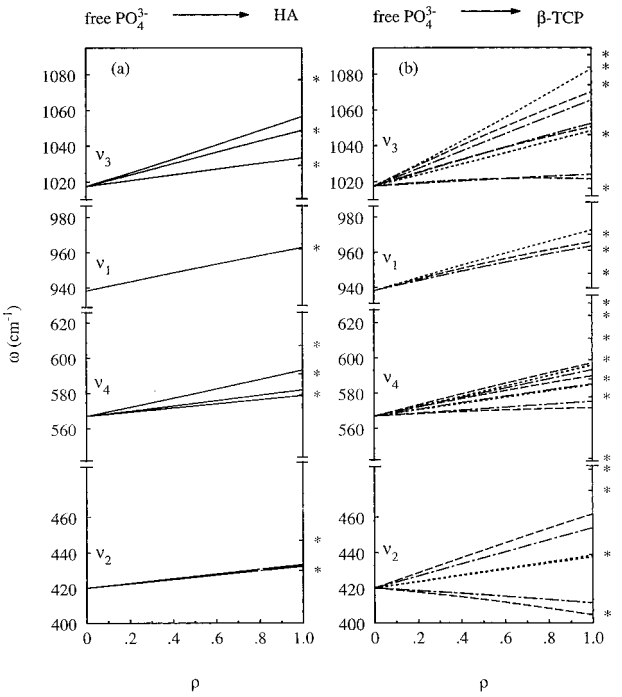

Figure 3. Energy splitting of the normal modes of a regular PO_4^{3-} tetrahedron ($\rho = 0$) as it is gradually distorted to the dimensions of the PO_4^{3-} ion in (a) HA and (b) β-TCP ($\rho = 1$). Dotted, dashed, and dashed−dotted lines correspond, respectively, to type-1, type-2, and type-3 tetrahedra of ref 16. Observed Raman frequencies are indicated on the right-hand side frequency axes by asterisks.

phonon energies in other II−IV−V_2 chalcopyrite compounds and their corresponding III−V zincblende analogues.[28] In this study it was also noted that the bending-to-stretching ratio could be assumed to be constant for all bonds in a series of II−IV−V_2 compounds. Considering the degree of covalency of the P−O bond in PO_4^{3-},[14] we may expect that the bond-length dependence of the force constants in PO_4^{3-} will not deviate substantially from that of tetrahedrally coordinated covalent crystals, and therefore we assume a d^{-4} scaling law for the force constants. Taking into account this force constant dependence and using the equilibrium atomic positions of the PO_4^{3-} groups in HA and β-TCP known from X-ray and neutron measurements,[9,16] eqs 1 and 2 allow us to calculate the vibrational frequencies of the distorted PO_4^{3-} groups. The equilibrium P−O bond length for the free PO_4^{3-} ion was taken to be 1.557 Å, a value not far from the average value of P−O bond lengths in β-TCP or HA, because this value reproduced well the shift of ≈20 cm^{-1} of the internal PO_4^{3-} bands of HA relative to the free ion values. This procedure to determine d_{PO} implicitly assumes that correlation effects are relatively unimportant for the symmetric stretching mode, which is a plausible assumption considering that the splitting of the ν_1 modes is not resolved in the HA spectrum shown in Figure 1a.

In Figure 3 we plot the evolution of the normal mode energies of the PO_4^{3-} tetrahedra as the oxygen atoms are gradually brought to their final positions relative to the central phosphorus corresponding to the HA (Figure 3a) and β-TCP (Figure 3b) crystal structures.

(24) Harrison, W. A. *Electronic Structure and the Properties of Solids: The Physics of the Chemical Bond*; Freeman: San Francisco, 1980.
(25) Buchenhauer, C. J.; Cardona, M.; Pollak, F. H. *Phys. Rev. B* **1971**, *3*, 1243.
(26) Buchenhauer, C. J.; Cardona, M. *Phys. Rev. B* **1971**, *3*, 2504.
(27) Pascual, J.; Pujol, J.; Artús, L.; Camassel, J. *Phys. Rev. B* **1991**, *43*, 9831.
(28) Artús, L.; Pascual, J. *J. Phys. Condens. Matter* **1992**, *4*, 5835.

In Figure 3b we have plotted the energies of the modes for the three different types of nonequivalent PO_4^{3-} ions which exist in β-TCP. Following the labeling of ref 16 we denote the nonequivalent PO_4^{3-} ions as types 1, 2, and 3. Although the model does not permit an accurate calculation of the values of the internal PO_4^{3-} frequencies, which is beyond the scope of this paper, it sheds light on the physical origin of the main differences observed between the internal Raman bands of HA and β-TCP, namely, the different number of observed peaks, the frequency spread of each band, and the larger width of some peaks in β-TCP. It can be seen that the lowering of the PO_4^{3-} symmetry in HA and β-TCP lifts the degeneracy of the doubly degenerate ν_2 as well as of the triply degenerate ν_3 and ν_4 modes.

The greater number of peaks observed in the Raman spectrum of β-TCP in relation to HA arises from the existence of three nonequivalent PO_4^{3-} tetrahedra in the β-TCP structure. The site field distortion acting on each nonequivalent tetrahedron gives rise to $3\nu_1$, $6\nu_2$, $9\nu_3$, and $9\nu_4$ different frequencies instead of the $1\nu_1$, $2\nu_2$, $3\nu_3$, and $3\nu_4$ of HA. These frequencies basically agree with the peaks observed in the Raman spectra of both compounds. In fact, for HA only one peak is found in the ν_1 region, and two peaks are observed in the ν_2 region. Although four peaks are detected in the ν_4 region, the peak at 615 cm^{-1} may be due to OH^- rotational modes, as already discussed. Also, in the ν_3 frequency region three main peaks are clearly distinguished, together with some other weaker peaks and shoulders which could be due to the correlation effects of the C_6 crystal field of HA. By contrast, two peaks and a shoulder can be observed in the ν_1 region of β-TCP.

In β-TCP, PO_4^{3-} tetrahedra of type 1 have nearly tetrahedral angles, and therefore the corresponding ν_2 bond-bending modes are almost degenerate. Also, for type-1 tetrahedra, two of the three ν_3 modes are nearly degenerate, as well as two of the three ν_4 modes. All these degeneracies can be related to the fact that three of the four P−O distances are equal in the type-1 tetrahedra. By contrast, in type-2 and type-3 tetrahedra all P−O distances are different, their relative differences ranging between 0.1% and 2.0%, resulting in the complete lifting of degeneracy of ν_2, ν_3, and ν_4 modes.

In the ν_2 region of the Raman spectrum of β-TCP three major broad peaks are detected which agree well with the calculated ν_2 mode splitting. In fact, although six modes should be expected in this region of the spectrum, from the model calculations shown in Figure 3b we can see that the frequencies of the ν_2 modes corresponding to the β-TCP distorted tetrahedra form three well-separated groups. As already discussed, the ν_2 modes of type-1 tetrahedra are nearly degenerate and form the central group at around 440 cm^{-1}. At either side we find the type-2 and type-3 ν_2 split modes, which are less than 7 cm^{-1} apart from each other, and may give rise to the observed doublet at 475−483 cm^{-1} and the broad peak at 405 cm^{-1}.

Similarly, two groups of frequencies can be distinguished in Figure 3b for the ν_4 modes of β-TCP. The lowest split ν_4 frequencies of type-2 and type-3 tetrahedra are found at around 573 cm^{-1}, whereas the rest of ν_4 frequencies appear closely spaced between 584 and 597 cm^{-1}. This grouping of frequencies agrees with the observed ν_4 bands of the Raman spectrum, where a doublet at 547−555 cm^{-1} is detected well separated from a group of closely spaced peaks between 578 and 631 cm^{-1}. The wider spread of frequencies of the experimental peaks in relation to the calculated values may be due to correlation effects, which could be important for the ν_4 modes as, according to our model, the energies of these modes in the distorted tetrahedra are very close to each other. The ν_3 modes display the largest dispersion, but their frequencies appear also grouped around three different regions. The lowest split ν_3 frequencies of type-2 and type-3 tetrahedra constitute a group around 1023 cm^{-1}. The two degenerate ν_3 modes of type-1 tetrahedra and one split ν_3 mode of each other type of tetrahedra form the central group around 1050 cm^{-1}, whereas the highest split ν_3 frequencies of each type of tetrahedra form a wider group between 1065 and 1083 cm^{-1}. This frequency distribution is reflected in the Raman spectrum of β-TCP in the ν_3 region, where three main peaks at 1016, 1048, and 1091 cm^{-1} are detected. The broad features of this band could be related to the existence of disorder in the β-TCP structure, whose effect may be enhanced by the higher sensitivity of the ν_3 modes to tetrahedron distortion and hence to disorder-induced fluctuations in the tetrahedron distortions.

As seen in Figure 3, and confirmed experimentally by the spectra of Figure 1, the internal PO_4^{3-} bands are significantly wider in β-TCP in relation to their counterparts in HA. This is particularly evident for the ν_2 and ν_4 bands, leading to a sizeable reduction of the gap between these bands, which is a characteristic difference between the Raman spectra of HA and β-TCP. In fact, as can be observed in Figure 3b, the modes corresponding to a specific tetrahedron type have a larger frequency dispersion than their counterparts in HA. This is a consequence of the greater distortion of bond lengths and angles in the β-TCP structure in comparison with HA.

3. External Modes: Ca^{2+} and PO_4^{3-} Lattice Modes and OH^- Modes. As already discussed in section III.A and paper 1, the modes occurring at frequencies below 320 cm^{-1} can be assigned to modes of translational character involving the Ca^{2+} and PO_4^{3-} sublattices, and to librational modes of the PO_4^{3-} groups. It can be seen in Figure 2 that Raman spectra of β-TCP and HA differ substantially in this frequency region. Whereas for HA several well-defined peaks are detected, only a band between 210 and 310 cm^{-1} and a broad peak centered at about 173 cm^{-1} are observed in the Raman spectrum of β-TCP. This fact can be related to the existence of disorder in the crystal structure of β-TCP. As discussed in paper 1, the β-TCP crystal is a crystallographically disordered structure which contain sites with partial occupancy and positional disorder of certain PO_4^{3-} groups. The structural disorder leads to a broadening of the lattice modes which produces a featureless Raman scattering band between 150 and 320 cm^{-1}. There is no Raman signal for β-TCP below 150 cm^{-1}. However, a well-defined peak is observed at 65 cm^{-1} in the Raman spectrum of HA, which as discussed in section III.A can be due to a Ca^{2+} lattice mode.

The most obvious difference between β-TCP and HA is the presence of the hydroxyl group in HA. The vibrational modes associated with the OH^- ion can be

used as a fingerprint for HA. As can be seen in Figure 2, in HA samples with high degree of crystallinity, the O−H stretching mode produces an intense Raman peak at 3576 cm^{-1} which is absent from β-TCP. Also, the translational modes of the OH^- sublattice produce a Raman peak at 335 cm^{-1} in the spectrum of HA, in a frequency region where no signal is detected in β-TCP. However, one should bear in mind that the detection of clear peaks associated with lattice and OH^- modes strongly depends on the degree of crystallinity of the sample. Also, one should be aware that hydration of the samples may produce Raman scattering signal at frequencies close to the hydroxyl stretching mode.

IV. Conclusions

We have compared the Raman spectra of polycrystalline HA and β-TCP in order to establish differences which allow to discern between these two calcium phosphates by means of Raman spectroscopy. Although these compounds give similar Raman spectra, which is basically dominated by the PO_4^{3-} internal modes, their different crystallographic structure gives rise to significant differences in their Raman spectra. The width of the Raman bands associated with the ν_2 and ν_4 internal modes of the PO_4^{3-} ion and their separation in frequency are characteristic features which can be easily observed even in samples with a high background noise level or poor crystallinity. Other differences, such as the overall number of peaks, the splitting of the ν_1 internal mode in β-TCP, the presence of modes associated with the hydroxyl ions in HA, and differences in the Ca^{2+} and PO_4^{3-} lattice modes have also been discussed, and may be used to confirm the identification. A dynamical model of the PO_4^{3-}, which takes into account short-range bond stretching and bond bending interactions as well as central electrostatic forces between the ions, has been set up and it was found to explain the main differences between the internal PO_4^{3-} bands of these compounds. The comparative study of the Raman spectra of HA and β-TCP has shown that currently available micro-Raman techniques, which allow a spatial resolution of about 1 μm, are capable of discerning between these two forms of calcium phosphate and therefore can be advantageously used as a nondestructive probe to study the microscopic structure of bioactive implant materials.

CM9604266